Eq. (18) in (A1) gives

$$\Gamma_\gamma=(2\pi)^3\sum_{m_0p}\int d\hat{k}_0(\hbar c/Vk_0)\{(-i)^L M_L^*(2L+1)^{1/2}\times\sum_M D_{Mp}^{(L)*}(\phi\theta 0)C(I_0LI_1;m_0Mm_1)+(-i)^{L+2}\times pE_{L+1}^*(2L+3)^{1/2}\sum_M D_{Mp}^{(L+1)*}(\phi\theta 0)C(I_0L+1I_1;m_0Mm_1)\}\{i^L M_L(2L+1)^{1/2}\sum_M D_{Mp}^{(L)}(\phi\theta 0)\times C(I_0LI_1;m_0Mm_1)+i^{L+2}pE_{L+1}(2L+3)^{1/2}\times\sum_M D_{Mp}^{(L+1)}(\phi\theta 0)C(I_0L+1I_1;m_0Mm_1)\}\rho(E_F).$$

Using the orthogonality relation for the D coefficients, given in (Ref. 8, p. 74),

$$\int d\hat{k}_0 D_{M'p}^{(L')*}(\phi\theta 0)D_{Mp}^{(L)}(\phi\theta 0)=[4\pi/(2L+1)]\delta_{MM'}\delta_{LL'},$$

we find

$$\Gamma_\gamma=8\pi k_0\{|M_L|^2\sum_{m_0M}C^2(I_0LI_1;m_0Mm_1)+|E_{L+1}|^2\sum_{m_0M}C^2(I_0L+1I_1;m_0Mm_1)\},$$
$$=8\pi k_0\{|M_L{}^2+|E_{L+1}|^2\},\qquad\text{(A2)}$$

the required relation.

PHYSICAL REVIEW VOLUME 171, NUMBER 2 10 JULY 1968

Time Dependence of Mössbauer Scattered Radiation*

P. THIEBERGER, J. A. MORAGUES,† AND A. W. SUNYAR
Brookhaven National Laboratory, Upton, New York

(Received 19 February 1968)

Time distributions of resonantly scattered 14.4-keV Fe^{57} γ rays were measured by using as time-zero signals the preceding 122-keV γ rays. A Co^{57} source coplated with Fe was used with two different metallic scatterers (2.54×10^{-3}-mm-thick 92.8% Fe^{57} and 4.53×10^{-3}-mm-thick 2.19% Fe^{57}) in a cylindrical geometry. Measurements were performed at different relative source velocities. From the measured time spectra, contributions due to random coincidences and to Rayleigh scattering were subtracted. A theory based on a classical model in which the scattering nuclei are represented by randomly situated harmonic oscillators was developed. The experimental results are compared with computed theoretical curves. Good agreement was found in most of the cases. Discrepancies observed in two instances are discussed.

I. INTRODUCTION

THE purpose of the present work is to measure the time spectrum of resonantly scattered γ rays and to develop a theory for this process based on a classical model. The first experimental results were reported previously.[1] It has been shown by Lynch *et al.*[2] that experimental results on the time distribution of Fe^{57} γ rays transmitted through a resonant absorber are well described by a theory in which each Fourier component of the incident radiation is changed in amplitude and phase according to a complex index of refraction. This complex index of refraction is given by the frequency response of the resonant oscillators in the absorber and by their number per unit volume. It can be written as[3]

$$n=[1+r(\omega_0{}'^2-\omega^2+i\omega\lambda)^{-1}]^{1/2}\simeq 1+\tfrac{1}{2}[r/(\omega_0{}'^2-\omega^2+i\omega\lambda)].\qquad(1)$$

Here, ω_0' and λ are the frequency and the decay constant of the oscillators in the absorber and r is a constant which contains the oscillator density.

It may perhaps seem surprising that it should be possible to describe the absorber by a macroscopic quantity in this case, where the wavelength of the 14.4-keV radiation of Fe^{57} is about three times smaller than the minimum distance between neighboring oscillators in a highly enriched Fe^{57} scatterer and about ten times smaller than the average distance in the case of a natural-iron scatterer. This can, however, be explained by the fact[4] that the average contribution modifying the incident wave at a point inside the absorber is due to the mutually in-phase, coherently forward scattered waves from the oscillators.

* Work performed under the auspices of the U.S. Atomic Energy Commission.

† Fellow of The Consejo Nacional de Investigaciones Científicas y Técnicas, Argentina. Permanent address: Comisión Nacional de Energía Atómica, Buenos Aires, Argentina.

[1] A. W. Sunyar, J. A. Moragues, and P. Thieberger, Bull. Am. Phys. Soc. **12**, 475 (1967).

[2] F. J. Lynch, R. E. Holland, and M. Hamermesh, Phys. Rev. **120**, 513 (1960).

[3] J. A. Stratton, *Electromagnetic Theory* (McGraw-Hill Book Co., New York, 1941), p. 321.

[4] J. Strong, *Concepts of Classical Optics* (W. H. Freeman and Company, San Francisco, 1958), p. 99.

The situation is different if scattering is to be studied at angles different from zero. There, the phase of the coherent contribution of each oscillator to the scattering in a given direction depends on its position. In addition, the noncoherent contributions to the scattering become important, while they cannot be seen in the case of transmission. Finally, since the direct radiation from the source does not reach the detector in the nonzero-angle scattering experiment, much more drastic changes in the time spectrum can be expected when the relative source velocity and/or scatterer thickness are changed.

Neuwirth[5] has measured the time distribution of x rays following internal conversion in an Fe^{57} scatterer. This author states that it would be impossible to measure the time distribution of scattered γ rays from a thick scatterer. It was known, however, from preliminary measurements by Sunyar and Kistner,[6] that such experiments were feasible.

The relation of the present work to the interpretation of measurements of magnetically perturbed angular distributions in resonant scattering[7] is also of interest.

II. THEORY

A. Coherent Scattering

For given incidence and scattering directions (or for a given point source and point detector) the time distribution of the coherently scattered radiation can be obtained by decomposing the incident wave packet into its Fourier components and adding coherently for each Fourier component the scattered contribution due to the response of all the oscillators. The scattered wave packet can then be reconstructed. In order to obtain the response of one oscillator to a given Fourier component, we could use (1) to calculate the amplitude and phase of this Fourier component at the position of this oscillator. We could again use (1) to calculate the change in phase and amplitude of the corresponding contribution to the scattered Fourier component. Finally, the experimental time distribution could be obtained by summing or averaging the partial time distributions over all possible incidence and scattering directions.

In order to simplify matters we perform the averaging before carrying out the detailed calculation. For this purpose we assume that we have N oscillators and call $A_j(\omega, x^j)$ the amplitude of the contribution to the ω component of the scattered wave due to the oscillator j. Here $x^j = x_1{}^j + x_2{}^j$, where $x_1{}^j$ and $x_2{}^j$ are the distances travelled by the wave in the scatterer before reaching and after leaving the oscillator j, respectively (see Fig. 1).

The relative phase Ψ_j of this contribution will be

$$\Psi_j = (1/c)\, n_{\mathrm{Re}}(\omega)\, \omega (x_1{}^j + x_2{}^j).$$

Here n_{Re} is the real part of the index of refraction (1). Since $n_{\mathrm{Re}}(\omega)$ only differs from unity by at most 10^{-5} and frequencies of interest only differ from ω_0' by at most one part in 10^{10}, we may write

$$n_{\mathrm{Re}}(\omega) = 1 + \epsilon_n(\omega),$$
$$\omega = \omega_0' + \epsilon_\omega,$$

so that

$$\Psi_j \simeq \omega_0'(x_1{}^j + x_2{}^j)/c + [\epsilon_\omega + \epsilon_n(\omega)\omega_0'](x_1{}^j + x_2{}^j)/c$$
$$= \Delta_j(x^j) + \varphi_j(\omega, x^j).$$

The phase may thus be considered as the sum of $\Delta_j(x^j)$, a very rapidly varying function of x^j, and $\varphi_j(\omega, x^j)$, which has a much slower variation with x^j.

The time distribution of the scattered radiation will then be

$$I(t) = \left\langle \left| \sum_{j=1}^{N} (2\pi i)^{-1} \int_{-\infty}^{+\infty} A_j(\omega, x^j)\, \exp[i\varphi_j(\omega, x^j)]\, \exp[i\Delta_j(x^j)]\, e^{i\omega t} d\omega \right|^2 \right\rangle_{\mathrm{av}}$$
$$= \left\langle \left| \sum_{j=1}^{N} \exp[i\Delta_j(x^j)]\, (2\pi i)^{-1} \int_{-\infty}^{+\infty} A_j(\omega, x^j)\, \exp[i\varphi_j(\omega, x^j)]\, e^{i\omega t} d\omega \right|^2 \right\rangle_{\mathrm{av}}. \quad (2)$$

If the average is now taken over an angular range small enough to maintain the values of the integrals essentially unchanged but large enough to make the $\Delta_j(x^j)$ vary in a way which can be considered random, then (2) reduces to

$$I(t) = \sum_{j=1}^{N} \left| (2\pi i)^{-1} \int_{-\infty}^{+\infty} A_j(\omega, x^j)\, \exp[i\varphi_j(\omega, x^j)]\, e^{i\omega t} d\omega \right|^2 \quad (3)$$

since the mean value of the modulus of the sum of N vectors with arbitrary phases is the quadratic sum of the individual moduli (problem of random walk).

In the above derivation an averaging over a considerable angular range is involved. One might think that a similar experiment in which the scattering angles are limited to a Bragg peak would lead to a different result. It is easy to show that this is not the case for a polycrystalline scatterer in which the microcrystals are sufficiently small so as to make extinction effects in each of them negligible. Under such circumstances, each microcrystal which contributes to the intensity in the Bragg peak will do so by the in-phase contribution of its nuclei and can be considered, for the purpose of performing the calculations, as a single oscillator. For different scattering events, different sets of microcrystals will contribute because of the divergence of the incident beam.

[5] W. Neuwirth, Z. Physik **197**, 473 (1966).
[6] A. W. Sunyar and O. C. Kistner (unpublished measurements).
[7] E. Ansaldo and L. Grodzins, Bull. Am. Phys. Soc. **12**, 546 (1967). E. Ansaldo, M.S. thesis, Massachusetts Institute of Technology, 1967 (unpublished).

It is over these sets that the average in (2) must now be taken. If these sets are labeled in a way so as to make roughly equal x^j correspond to the same j then we see that (3) is again obtained.

Since the dependence of $A_j(\omega, x^j)$ and $\varphi_j(\omega, x^j)$ on x^j is a slow one and since we have a large number of uniformly distributed oscillators we can now replace the sum in (3) by the corresponding integral

$$I(t)=D\int_0^{x_{1\,\max}}\left|\int_{-\infty}^{+\infty}A(\omega,x)e^{i\varphi(\omega,x)}e^{i\omega t}d\omega\right|^2 dx_1, \quad (4)$$

where D is a constant proportional to the number of oscillators per unit volume and to the area of the scatterer.

In order to evaluate this integral we must now write in an explicit form the Fourier component $A(\omega, x)e^{i\varphi(\omega,x)}e^{i\omega t}$. As has been said above, this component will be given by the corresponding component of the incident, exponentially damped radiation $e^{i\omega t}/[i(\omega-\omega_0)+\frac{1}{2}\lambda]$ modified by a resonant absorber thickness x_1, by the response of the oscillator, and finally by a resonant absorber thickness x_2. According to Ref. 2 and to the well-known expression for the response of a resonant damped oscillator, this Fourier component is proportional to

$$\frac{e^{i\omega t}}{i(\omega-\omega_0)+\frac{1}{2}\lambda}\exp\left(-i\frac{1}{2}\frac{\omega_0'}{c}\frac{r}{\omega_0'^2-\omega^2+i\omega\lambda}x_1\right)$$

$$\times(\omega_0'^2-\omega^2+\lambda i\omega)^{-1}\exp\left(-i\frac{1}{2}\frac{\omega_0'}{c}\frac{r}{\omega_0'^2-\omega^2+i\omega\lambda}x_2\right) \quad (5)$$

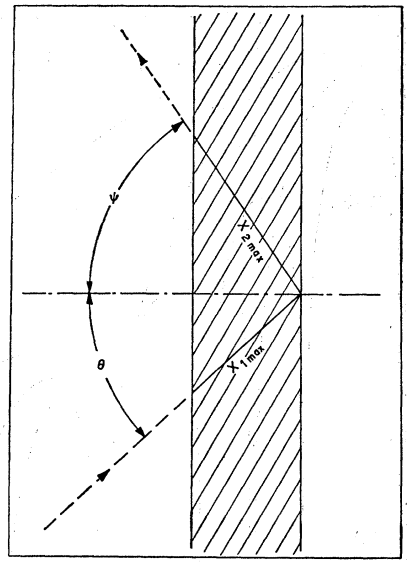

FIG. 1. Schematic representation of a scatterer. θ and ψ are the incidence and scattering angles respectively. The incidence and scattering directions are generally not coplanar.

An additional phase shift $\epsilon_\omega(x_1+x_2)/c$ has been neglected, since, for the largest values of (x_1+x_2) and ϵ_ω of interest, its value is $\leq 10^{-5}$ rad.

As usual, we write $\omega_0'^2-\omega^2\simeq 2\omega_0'(\omega_0'-\omega)$. Equation (4) then becomes

$$I(t)=E\int_0^{x_{1\,\max}}\left|\int_{-\infty}^{+\infty}\frac{e^{i\omega t}\exp\{(i/4c)[rx/(\omega-\omega_0'-\frac{1}{2}i\lambda)]\}}{(\omega-\omega_0-\frac{1}{2}i\lambda)(\omega-\omega_0'-\frac{1}{2}i\lambda)}d\omega\right|^2 dx_1, \quad (6)$$

where $E=D/4\omega_0'^2$. Performing the integrals (see Appendix) and setting $\omega_0-\omega_0'=\Delta\omega$ and $B=r(x_{1\,\max}+x_{2\,\max})/c$, Eq. (6) yields

$$I(t)=[2\cos\Psi/(\cos\Psi+\cos\theta)]Ee^{-\lambda t}t\{1-\sum_{N=0}^{+\infty}[(-1)^{N+1}/(2N+1)][\Delta\omega^2(4t/B)]^N\sum_{m=1}^{2N+1}(-1)^m$$

$$\times[J_{2N+1-m}(B^{1/2}t^{1/2})J_{m-1}(B^{1/2}t^{1/2})+J_{2N+2-m}(B^{1/2}t^{1/2})J_m(B^{1/2}t^{1/2})]\}, \quad (7)$$

where θ and Ψ are the incidence and scattering angles, respectively, with respect to the normal to the scatterer (Fig. 1). For the special case of $\Delta\omega=0$, (7) reduces to

$$I(t)=[2\cos\Psi/(\cos\Psi+\cos\theta)]Ee^{-\lambda t}t[1-J_0^2(B^{1/2}t^{1/2})-J_1^2(B^{1/2}t^{1/2})]. \quad (8)$$

For very thick scatterers this function is of the form $te^{-\lambda t}$ and for very thin scatterers it approaches the form $t^2e^{-\lambda t}$. For large values of $\Delta\omega^2 4t/B$, the series (7) does not converge or converges very slowly and it is convenient to use the following expression for $I(t)$ (see Appendix):

$$I(t)=2[\cos\Psi/(\cos\Psi+\cos\theta)]\tfrac{1}{4}E(e^{-\lambda t}B/\Delta\omega^2)\{1+\sum_{N=0}^{+\infty}(-1)^N(B/\Delta\omega^2 4t)^N[(2N+1)^{-1}\sum_{m=0}^{2N}(-1)^m$$

$$\times(J_m(B^{1/2}t^{1/2})J_{2N-m}(B^{1/2}t^{1/2})+J_{2N-m+1}(B^{1/2}t^{1/2})J_{m+1}(B^{1/2}t^{1/2}))$$

$$-[2(2N+2)/t\Delta\omega]\sin(B/4\Delta\omega+t\Delta\omega)J_{2N+2}(B^{1/2}t^{1/2})-4(2N+1)(Bt)^{-1/2}\cos(B/4\Delta\omega+t\Delta\omega)J_{2N+1}(B^{1/2}t^{1/2})]\}. \quad (9)$$

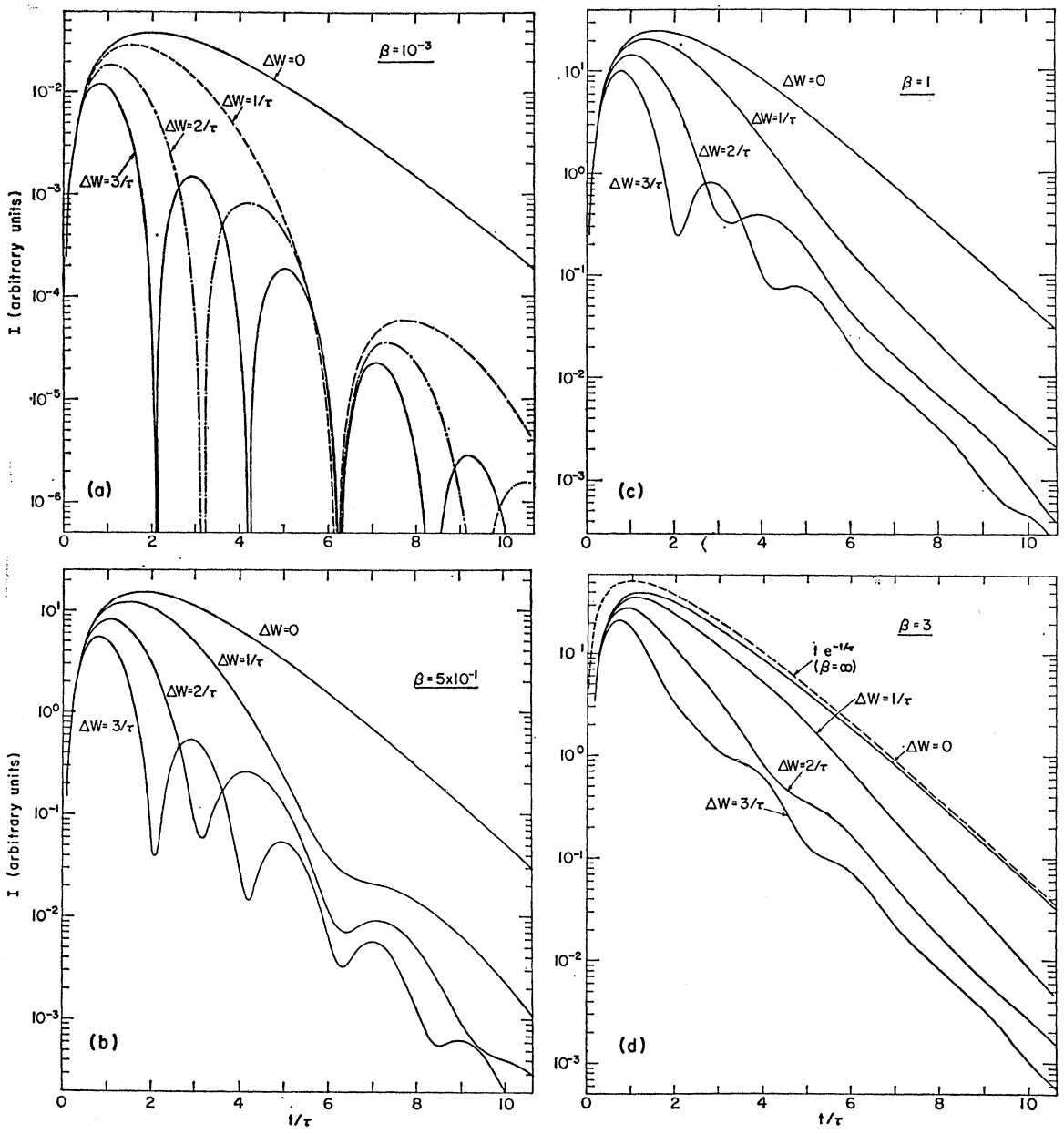

FIG. 2. Curves showing the time dependence of resonantly scattered radiation, as obtained from Eqs. (7) and (9). The curves were computed for frequency shifts $\Delta\omega=0$, $1/\tau$, $2/\tau$, and $3/\tau$, where $\tau=1/\lambda$ is the mean life of the excited state. Cases which correspond to four different values of the thickness parameter are shown. These curves contain an arbitrary normalization factor which is identical for all. In Fig. 2(a), the curve for $\Delta\omega=0$ coincides for all practical purposes with the functional form $t^2e^{-t/\tau}$, a result which would be obtained in the limit $\beta\to 0$. In Fig. 2(d) the limiting case for $\beta=\infty$ is indicated. This result does not depend on the value of $\Delta\omega$.

Neuwirth[5] has obtained expressions similar to (7) and (9) for the time distribution of x rays following internal conversion in the scatterer. For the case of scattered rays and $\Delta\omega=0$, however, this author gives a formula which is not in agreement with our expressions nor with our experimental result.

In Fig. 2 the time dependences corresponding to different combinations of scatterer thicknesses and source velocities are shown. These curves were obtained from (7) and (9) by means of a computer program. The parameter β characterizes the effective scatterer thickness and its value is

$$\beta=B/2\lambda=\tau(x_{1\,\max}+x_{2\,\max})/2c\lambda.$$

When $x_{1\,\max}=x_{2\,\max}$ and the source velocity is zero, $e^{-\beta}$

is the transmission through the scatterer at the center of the line.

The spectral distribution of the scattered radiation was also calculated. The intensity $I(\omega)$ will be given by

$$I(\omega)=\langle|\sum_{j=1}^{N}A_j(\omega,x^j)\exp[i\varphi_j(\omega,x^j)]\exp[i\Delta_j(x^j)]|^2\rangle_{\text{av}}.$$

Since the phases are considered to vary at random with varying incidence and scattering angles over which the average is taken,

$$I(\omega)$$

$$=\sum_{j=1}^{N}|A_j(\omega,x^j)|^2$$

$$\simeq\frac{D}{4\omega_0'^2}\int_0^{x_{1\max}}\left|\frac{\exp\{-\lambda rx/8c[(\omega-\omega_0')^2+\frac{1}{4}\lambda^2]\}}{(\omega-\omega_0'-\frac{1}{2}i\lambda)(\omega-\omega_0-\frac{1}{2}i\lambda)}\right|^2dx_1.$$

This becomes

$$I(\omega)=2\cos\Psi/(\cos\Psi+\cos\theta)F[(\omega-\omega_0)^2+\tfrac{1}{4}\lambda^2]^{-1}$$
$$\times\{1-\exp(-\lambda B/4[(\omega-\omega_0')^2+\tfrac{1}{4}\lambda^2])\},\quad(10)$$

where $F=Dc/\omega_0'^2r\lambda$.

It is interesting to point out that the Fourier transform of the time distribution (7) and (9) would not give the result obtained in (10). So for instance (10) gives a natural line shape for $B\to\infty$ while the corresponding time distribution is $te^{-t/\tau}$.

B. Incoherent Scattering

Two kinds of incoherent processes, where the incoming and outgoing radiations differ in frequency, will also contribute to the observed scattered intensity. In the first, energy is transferred to the lattice of the scatterer. In the second, after the scattering process, one of the nuclei in the scatterer is left in a different m substrate.

A classical model for the first type of process can be obtained with the same approach used to describe the emission from a Mössbauer source.[8–10] These authors describe the emitting nucleus as performing sinusoidal oscillations due to the lattice vibrations. As a consequence, the emitted Fourier spectrum is split into an unshifted line representing the recoil-free fraction (f), and satellite lines corresponding to the energy-shifted fraction ($1-f$). Only the unshifted component of the radiation from the source will interact appreciably with the scattering nuclei. These nuclei also have to be considered as performing the same type of sinusoidal vibrations.

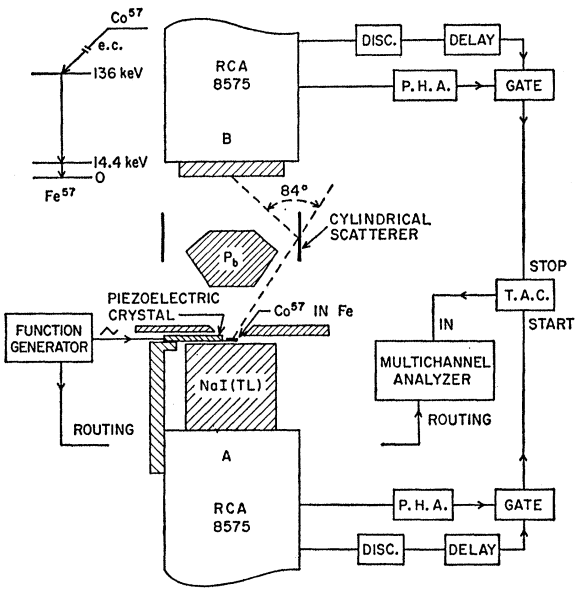

FIG. 3. Geometry of the experimental arrangement and simplified block diagram of the electronic equipment. P.H.A. indicates a single-channel pulse-height analyzer and T.A.C. indicates a time-to-amplitude converter. Not shown is a gate generator (actuated by the function generator) which blocked storage in the multichannel analyzer during the first 20 msec following each turning point of the velocity transducer.

In a system of coordinates fixed to a scattering nucleus the unshifted radiation from the source is again split into a central component and satellite lines (this accounts for the factor f' entering in the expression for the scattering cross section). It is this last unshifted component seen by the scattering oscillator which induces the forced oscillations. The Fourier spectrum of this component has the same shape as would be seen by an oscillator at rest, placed at the same point. Therefore the response of the oscillator will have the same time dependence as in Sec. IIA where no lattice vibrations were considered.

With respect to a system of coordinates fixed to the laboratory the Fourier spectrum emitted by this oscillator will have a central unshifted line and satellite lines, all of which will contribute to the measured intensity. The unshifted component will interact with the resonant scatterers while leaving the scatterer. Its time dependence will be the one which has been obtained in Sec. IIA. The shifted components will leave the scatterer without further resonant interactions. Their time dependence can therefore be obtained from Sec. IIA by setting $B=rx_{1\max}/c$ and by eliminating the factor $2\cos\Psi/(\cos\Psi+\cos\theta)$ in Eqs. (7) and (9). In the same way, the spectral distribution can be obtained from (10).

For the second type of incoherent process no classical model was found. It is, however, thought to be, in principle, not too different from the above-discussed first type. In fact, in one case it is the lattice and in the other it is one nucleus which changes its quantum state. The

[8] F. L. Shapiro, Usp. Fiz. Nauk **72**, 685 (1960) [English transl.: Soviet Phys.—Usp. **3**, 881 (1961)].

[9] J. Van Kranendonk, in *Proceedings of the Seventh International Conference on Low Temperature Physics, 1960*, edited by G. M. Graham and A. C. Hollis-Hallett (University of Toronto Press, Toronto, 1961), pp. 9–20.

[10] H. Frauenfelder, *The Mössbauer Effect* (W. A. Benjamin, Inc., New York, 1963), pp. 17–20.

TABLE I. Different types of events which take place in the emission and subsequent scattering of γ rays in a situation where recoil-free resonant processes are possible. In the last two columns the presence or absence of resonant absorption in the scatterer is indicated.

Radiation from source		Scattering		Resonant absorption in scatterer	
				Ingoing	Outgoing
Recoil-free	Mössbauer	Coherent	(a) Recoil-free without change in ground substate	yes	yes
		Incoherent	(b) With recoil	yes	no
			(c) Recoil-free with change in ground substate	yes	yes
	Rayleigh	Coherent	(d) Recoil-free	yes	yes
		Incoherent	(e) with recoil	yes	no
With recoil	Rayleigh	Incoherent and coherent	(f) With and without recoil	no	no

time and spectral distributions corresponding to this second type of process are therefore assumed to be the same as for the first type.

III. EXPERIMENTAL ARRANGEMENT

In Fig. 3 the geometry of the experimental arrange ment is shown schematically and a simplified block diagram of the electronic equipment is given.

The 122-keV γ rays from the Co^{57}-in-Fe source are detected in detector A and provide the time-zero pulses which are the start signals for the time-to-amplitude converter. 14.4-keV γ rays, which follow the emission of the 122-keV γ rays and are scattered by the iron scatterer, are detected in detector B. These signals produce the stop pulses for the time-to-amplitude converter. Thus the spectrum obtained in the multichannel analyzer will follow the probability distribution corresponding to the observation of a scattered photon in given time intervals after the excited state in the source is formed.

Detector A consisted of a 38.1-mm-diam and 25.4-mm-thick NaI(Tl) crystal mounted on a RCA 8575 photomultiplier tube. Detector B had a quartz window and used the same type of photomultiplier tube. The NaI(Tl) crystal was 44.5 mm in diameter and 6 mm thick.

The source was prepared by coplating carrier-free Co^{57} with natural Fe onto a Cu foil. The source intensity was adjusted to about 10^5 dis/sec. The velocity absorption spectrum of this source was measured with a natural-iron absorber. The linewidth, after correction for the absorber thickness, was found to be within 11% of the value corresponding to natural linewidth. In order to detect any possible effect on the time distribution due to self-absorption in the source, a study of the decay curve of the 14.4-keV state was performed. This was done by using the arrangement of Fig. 3 with the scatterer and Pb shield removed. No such effect was found with the present source. A value of 97 ± 1 nsec was obtained for the half-life, in agreement with previous results.[11]

[11] See listings by A. H. Muir, Jr., K. J. Ando, and H. M. Coogan, in *Mössbauer Effect Data Index, 1958–1965* (Interscience Publishers, Inc., New York, 1966).

The source was mounted on a simple and compact velocity drive consisting of a piezoelectric ceramic "Bender" ("Bimorph" [12]). A triangular voltage wave form from a precision function generator was applied to this transducer. The range of frequencies used during the experiments was from 0 to 4 cps and the peak value of the voltage was about 30 V. The response of the velocity drive was studied using an optical system. A beam of light was modulated by means of a slit with one of its edges fixed to the velocity drive, with the other one stationary. The beam intensity was measured with a photomultiplier tube connected to an oscilloscope. In order to reduce spurious oscillations observed after the turning points it was necessary to rigidly attach to the velocity drive a damping device consisting of a small plate submerged in mineral oil. After this was done, deviations from linearity could only be seen within the first 20 msec following each turning point. During these periods the analyzer was gated off by pulses derived from the function generator. An amplitude calibration of the velocity drive was performed with a microscope.

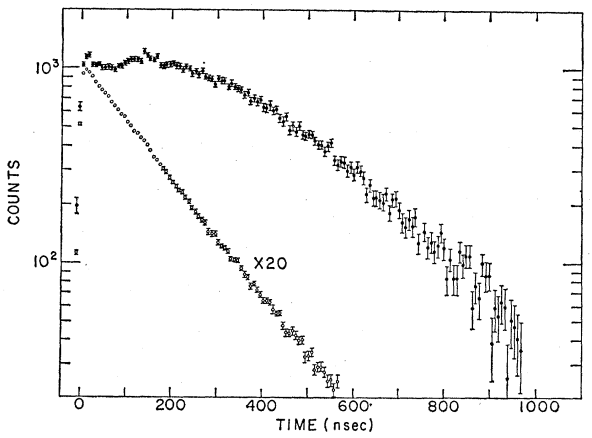

FIG. 4. Shown are the data obtained in a time-distribution measurement carried out at zero relative velocity with the natural-iron scatterer. Also shown is a conventional delayed coincidence curve of the 14.4-keV level in Fe^{57}. Random coincidences have been subtracted in both cases.

[12] Clevite Corporation.

Two cylindrical scatterers were used during these experiments. The first consisted of a 92.8%-enriched Fe^{57} foil, 2.54×10^{-2} mm thick and 20 mm high, supported by a paper cylinder. The second was made of natural iron (2.19% Fe^{57}) 4.53×10^{-3} mm thick and 65 mm high. This scatterer was self-supporting and was mounted between two solid rings which were not reached by the γ rays from the source.

To reduce possible vibrations, the whole system was shock mounted. To make certain that no vibrations of the thin natural-Fe scatterer remained, an absorption velocity spectrum was measured in which the scatterer mounted in the same position as during the scattering experiments was used as an absorber. No line broadening was observed.

In order to obtain the best possible time resolution it is necessary to set the discrimination levels of the fast discriminators partially within the region of noise. In the present experiment, the counting rate from detector A was rather high. If the unwanted signals were to reach the time-to-amplitude converter (as would be the case in a conventional fast-slow system) a serious dead-time problem would arise. For this reason the system shown in Fig. 3 was adopted.

"Prompt" curves were measured with annihilation radiation. In these runs the channel positions were kept at the values corresponding to the 14.4- and 122-keV photopeaks. The observed full width at half-maximum was 7 nsec. It was verified that this width was not affected by the high counting rate in detector A by placing the Co^{57} source on the velocity drive and preventing the 14.4-keV γ rays from reaching detector B by means of an absorber.

The time calibration of the time-to-amplitude converter was obtained with a Tektronix RM 181 time mark generator and an oscilloscope.[13]

IV. EXPERIMENTAL RESULTS AND COMPARISON WITH THEORY

An example of the data obtained in a time-distribution measurement performed with the natural-Fe scatterer at zero relative velocity is shown in Fig. 4, together with a decay curve of the 14.4-keV level in Fe^{57}. Random coincidences were subtracted from both spectra. In this case the ratio of real to random coincidences at the maximum of the scattering curve was about 8.

To compare the experimental results with the theory it is necessary to take into account the fact that scattering processes other than Mössbauer scattering (mainly Rayleigh scattering) also contribute to the observed intensity. Different combinations of emission and scattering, both with and without recoil, either leaving or not leaving the scattering nucleus in its original ground substate, must be considered (see Table I). Other factors which enter into the interpreta-

[13] P. Thieberger, Arkiv Fysik **22**, 127 (1962).

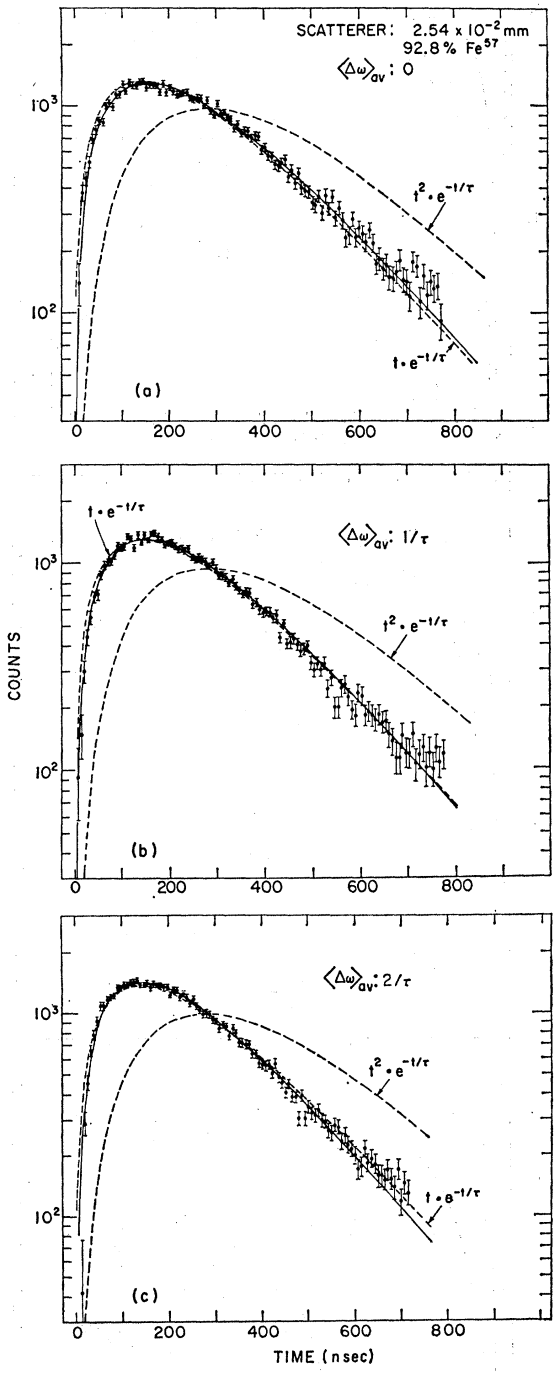

FIG. 5. Time spectra of resonantly scattered γ rays obtained with the 2.54×10^{-2}-mm-thick, 92.8% Fe^{57} scatterer. In Figs. 5(a)–5(c) the data collected at source velocities which correspond to average frequency shifts $\langle\Delta\omega\rangle_{av}=0$, $1/\tau$, and $2/\tau$ are shown. Random coincidences and contributions due to Rayleigh scattering have been subtracted. The solid curves have been computed from the theory (see text). The dashed curves which have the functional forms $te^{-t/\tau}$ and $t^2e^{-t/\tau}$, are normalized to the area of the experimental points and are shown for purposes of comparison.

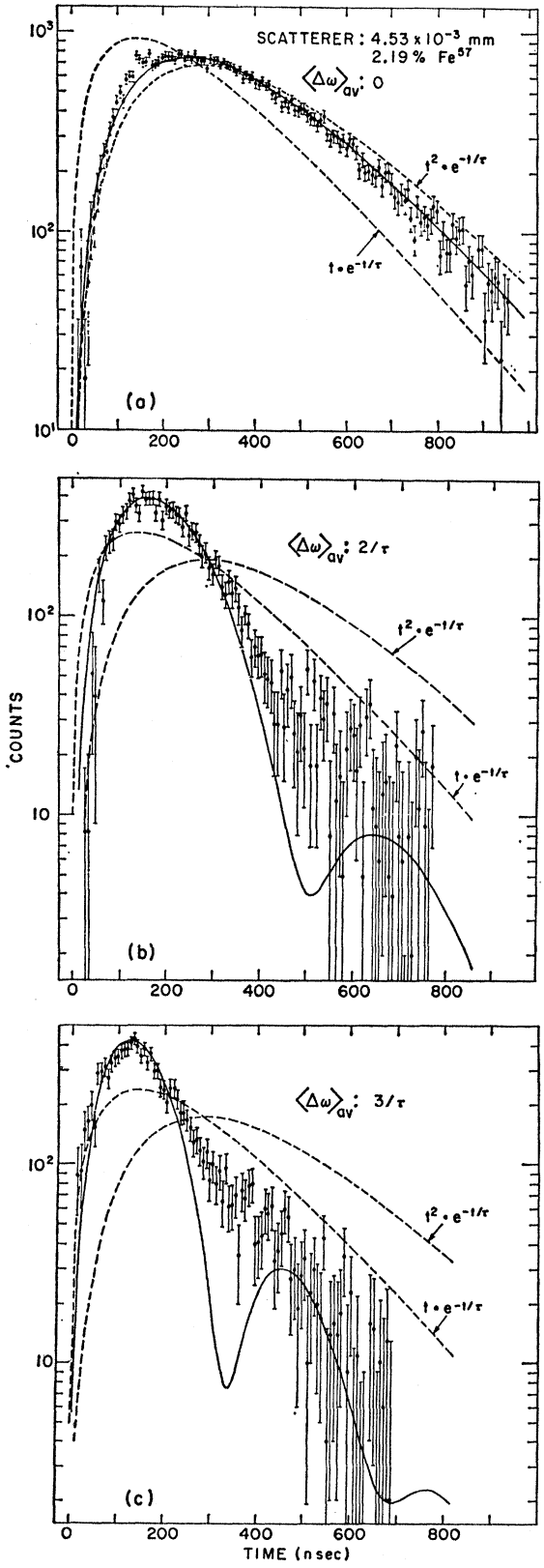

Legend for Fig. 6 in opposite column.

tion of the results include the splitting of the emission and scattering spectra, the angular distributions in the scattering processes, and the finite sizes of the scatterer and detector. Finally, a correction due to nonresonant absorption in the scatterer is introduced.

A computer program was written in order to apply the results of Sec. II to the cases (a), (b), and (c) of Table I. This program performs a numerical integration over the geometrically allowed incidence and scattering angles and the corresponding values of $\Delta\omega$. Angular correlations corresponding to the transitions to and from the different substates, computed by assuming a random distribution of magnetic field directions in the scatterer, are taken into account. In addition, the presence of nonresonant absorption, which is not included in Eqs. (7) and (9), was introduced numerically in these calculations and resulted in very small corrections for our scatterers.

Modifications of the angular correlations due to preferential scattering at Bragg angles and to possible angular variation of the scattering f factor were not taken into account.

For cases (d), (e), and (f) of Table I a similar program was used. These processes differ from those described in Sec. II in that the Fourier spectrum is not modified by the Rayleigh scattering. The contribution to the time spectrum due to (f) is obviously a pure exponential. Deviations from an exponential were found in cases (d) and (e). However, a summing of the time spectra (d), (e), and (f), weighted with their corresponding intensities, showed that these deviations were sufficiently small to be neglected.

Interference effects between cases (a) and (d) were also neglected. This is certainly justified for the natural-iron scatterer where most of the Rayleigh scattering is produced by Fe^{56} nuclei not capable of resonant scattering. In the case of the enriched scatterer, the relative intensity of (d) with respect to (a) is smaller. For $\Delta\omega=0$ the ratio of these intensities is only about 8%.

The separations of the hyperfine components in the source and in the scatterer are large compared to the linewidth. Any contribution to the scattering due to partial overlap of adjacent hyperfine lines is very small, even for a frequency shift of $\Delta\omega=3/\tau$. Such effects were therefore neglected.

A certain exponential contribution due to Rayleigh scattering was subtracted from the experimental data. For each measurement with the enriched scatterer, the magnitude of this contribution as well as the normaliza-

FIG. 6. Time spectra of resonantly scattered γ rays obtained with the 4.53×10^{-3}-mm-thick, natural-Fe scatterer. In Figs. 6(a)–6(c) the data collected at source velocities which correspond to average frequency shifts $\langle\Delta\omega\rangle_{av}=0$, $2/\tau$, and $3/\tau$ are shown. Random coincidences and contributions due to Rayleigh scattering have been subtracted. The solid curves have been computed from the theory (see text). The dashed curves, which have the functional forms $te^{-t/\tau}$ and $t^2e^{-t/\tau}$, are normalized to the area of the experimental points and are shown for purposes of comparison.

TABLE II. Relations between Rayleigh scattering intensities (R), and Mössbauer scattering intensities (M) for all the measured cases. The "expected" values in the first column were obtained from separate measurements (see text) and the corresponding values in the other columns were computed from the theory.

Scatterer	Intensity ratios	$R/M(\langle\Delta\omega\rangle_{av}=0)$	$\frac{R/M(\langle\Delta\omega\rangle_{av}=1/\tau)}{R/M(\langle\Delta\omega\rangle_{av}=0)}$	$\frac{R/M(\langle\Delta\omega\rangle_{av}=2/\tau)}{R/M(\langle\Delta\omega\rangle_{av}=0)}$	$\frac{R/M(\langle\Delta\omega\rangle_{av}=3/\tau)}{R/M(\langle\Delta\omega\rangle_{av}=0)}$
Enriched Fe^{57}	observed	0.197	1.4	1.5	
	expected	0.142	1.2	1.6	
Natural Fe	observed	0.485		3.0	3.3
	expected	0.488		3.8	7.4

tion factor for the computed theoretical curve was obtained by means of a least-squares fitting program. No other parameters were left open in the fitting procedure. The results corresponding to average frequency shifts $\langle\Delta\omega\rangle_{av}=0$, $1/\tau$, and $2/\tau$ are shown in Fig. 5. For comparison the functions $te^{-t/\tau}$ and $t^2e^{-t/\tau}$ are also shown with their areas normalized to the experimental points. The effective thickness of the present scatterer is very large and the theoretical curves would for all practical purposes coincide with the function $te^{-t/\tau}$. The small differences seen in Fig. 5 are entirely due to the introduction of nonresonant absorption. The measuring time for each of these experiments was about two weeks.

With the nonenriched scatterer, it was not necessary to use a least-squares fitting procedure to determine the amount of Rayleigh scattering. The exponential contribution was easily seen in the experimental data and could be subtracted with sufficient accuracy. The only adjustable parameters were the normalization factors for the theoretical curves and they were obtained by least-squares fitting. The results for average frequency shifts of $\langle\Delta\omega\rangle_{av}=0$, $2/\tau$, and $3/\tau$ are shown in Fig. 6. The measuring time was from about three to six weeks for each of these experiments.

The relations between the resulting intensities of resonant and nonresonant contributions to the time spectra for all of our measurements are compared with "expected" values in Table II. The "expected" values shown in the first column were obtained by performing a separate measurement in which the scattering intensity at $\langle\Delta\omega\rangle_{av}=0$ was compared with the scattering intensity at very large $\Delta\omega$. The intensities of Rayleigh and Mössbauer scatterings for $\langle\Delta\omega\rangle_{av}=0$ were obtained by taking into account the computed reduction in the Rayleigh scattering intensity due to resonant absorption. The "expected" values of columns 2, 3, and 4 were computed with the above-mentioned programs.

V. DISCUSSION AND CONCLUSIONS

It is not too surprising to find that a classical theory of the type presented in Sec. II is rather successful in describing the experimental results of Sec. IV. A similar result was found[2] for the time spectra of radiation transmitted through a resonant absorber. In this latter case, a quantum-mechanical calculation[14] has confirmed the classical results. A certain degree of *a priori* justification for the classical procedure can be found in the possibility of describing photons by "associated classical fields."[15–17]

Several attempts have been made to explain the discrepancies between theory and experiment observed for the natural-Fe scatterer at $\langle\Delta\omega\rangle_{av}=2/\tau$ and $3/\tau$ (see Fig. 6 and Table II). Theoretical curves corresponding to these cases were computed by assuming line broadening as large as 20%. A 20% line broadening is about twice the experimentally permissible limit. No substantial improvement of the fits was obtained by this procedure. These discrepancies might also be caused by the presence of "satellite" lines close to the zero-velocity line. However, no deviation from the expected line shape was observed in absorption spectra obtained by using the scatterer foil as an absorber. If such satellite lines are present, their intensity is too small to account for the discrepancies. Finally, the possibility that the contribution (b) or (c) (Table I) to the time spectrum could be different from the result obtained in Sec. II was considered. It was assumed that in one or the other of these cases the absorption and subsequent reemission of the γ rays in the scatterer are separate processes. Even though the fits for the last two cases of Fig. 6 were improved, the good agreement obtained in all the other cases was completely destroyed. This possibility can therefore be ruled out as an explanation of the discrepancies. It is thus likely that the incoherent resonant scattering processes contribute to the time spectrum in a way similar to that of the coherent processes.

The observed discrepancies therefore remain unexplained. Their presence implies that the scattered radiation contains Fourier components with amplitudes different from the theoretically expected ones. It is possible that this effect is of the same type as the one observed by Lennuier[18] in his studies of the resonant scattering of light. In his experiments the scattered spectrum contained frequencies centered on the reso-

[14] S. M. Harris, Phys. Rev. **124**, 1178 (1961).
[15] G. Beck, Nuovo Cimento **1**, 70 (1955).
[16] L. M. Falicov, Nuovo Cimento **16**, 247 (1960). [See also G. Beck, *ibid.* **19**, 825 (1961)].
[17] L. Menegozzi, Nuovo Cimento, Suppl. **4**, 15 (1966).
[18] R. Lennuier, Ann. Phys. (Paris) **2**, 233 (1947).

nance even though these frequencies were absent from the incident radiation.

It would be of interest to perform an experiment in which the absorption spectra of resonantly scattered γ rays derived from a source which moves at different velocities are analyzed by means of a resonant absorber. The manner and extent to which such experimental results deviate from expectations based on Eq. (10) could provide more insight into the deviations observed in the present experiment.

Several possible interpretations of magnetically perturbed angular distribution measurements in resonant scattering have been discussed.[7] One such interpretation, in which the excitation and decay of the excited state in the scatterer are considered as independent processes, is ruled out by our results.

ACKNOWLEDGMENTS

We wish to thank Dr. A. Schwarzschild and Dr. O. C. Kistner for the loan of equipment and for interesting comments. It is a pleasure to acknowledge stimulating discussions with Dr. M. Blume and Dr. E. Church. One of us (J.A.M.) gratefully acknowledges the opportunity of working at this Laboratory. He would also like to thank the Consejo Nacional de Investigaciones Científicas y Técnicas for a fellowship and the Comisión Nacional de Energía Atómica for granting him leave of absence.

APPENDIX

The integral of Eq. (6),

$$I(t)=E\int_0^{x_{1\max}}\left|\int_{-\infty}^{+\infty}\frac{e^{i\omega t}\exp\{(i/4c)[rx/(\omega-\omega_0'-\frac{1}{2}i\lambda)]\}}{(\omega-\omega_0-\frac{1}{2}ix)(\omega-\omega_0'-\frac{1}{2}i\lambda)}\,d\omega\right|^2 dx_1, \tag{A1}$$

was evaluated as follows:

The integral with respect to ω can be evaluated by finding the residues of the integrand in the complex ω plane, as in Ref. 2. Setting $b=rx/4c$, we have

$$\oint\frac{e^{i\omega t}\exp[ib/(\omega-\omega_0'-\frac{1}{2}i\lambda)]}{(\omega-\omega_0-\frac{1}{2}i\lambda)(\omega-\omega_0'-\frac{1}{2}i\lambda)}\,d\omega=\oint_{\omega_0+i\lambda/2}G\,d\omega+\oint_{\omega_0'+i\lambda/2}G\,d\omega=I_1+I_2. \tag{A2}$$

In the first integral we put $z=\omega-\omega_0-\frac{1}{2}i\lambda$:

$$I_1=\exp[(i\omega_0-\tfrac{1}{2}\lambda)t]\oint_{z=0}\frac{e^{izt}}{z}\frac{\exp[ib/(z+\omega_0-\omega_0')]}{z+\omega_0-\omega_0'}\,dz=\frac{\exp\{i[\omega_0 t+b/(\omega_0-\omega_0')]-\frac{1}{2}\lambda t\}}{\omega-\omega_0'}. \tag{A3}$$

In the second integral we put $z=\omega-\omega_0'-\frac{1}{2}i\lambda$:

$$\begin{aligned}I_2&=\exp[(i\omega_0'-\tfrac{1}{2}\lambda)t]\oint_{z=0}\frac{e^{i(zt+b/z)}}{z}\frac{dz}{z+\omega_0'-\omega_0}\\&=-\exp[(i\omega_0'-\tfrac{1}{2}\lambda)t]\oint_{z=0}\sum_{n=0}^{+\infty}\frac{z^{n-1}}{(\omega_0-\omega_0')^{n+1}}\,e^{i(zt+b/z)}dz.\end{aligned} \tag{A4}$$

The formula for generating Bessel functions,

$$\exp[\tfrac{1}{2}Y(U-U^{-1})]=\sum_{l=-\infty}^{+\infty}U^l J_l(Y),$$

is used to write

$$e^{i(zt+b/z)}=\sum_{m=-\infty}^{+\infty}im(t/b)^{m/2}z^m J_m(2b^{1/2}t^{1/2}).$$

After substitution into Eq. (A4), the only nonzero residues are those for which $n=-m$. As a result one obtains

$$I_2=-\exp[(i\omega_0'-\tfrac{1}{2}\lambda)t]\sum_{n=0}^{+\infty}\frac{(ib)^n}{(\omega_0-\omega_0')^{n+1}}(bt)^{-n/2}J_n(2b^{1/2}t^{1/2}), \tag{A5}$$

$$I_2=-\exp[(i\omega_0'-\tfrac{1}{2}\lambda)t]\Big[\sum_{n=-\infty}^{+\infty}S_n-\sum_{n=-\infty}^{-1}S_n\Big]. \tag{A5'}$$

If we again use the formula for generating Bessel functions, we can cancel I_1 [Eq. (A3)]. Equation (A1) then becomes

$$I(t)=E\int_0^{x_{1\,\max}}\left|\frac{\exp[(i\omega_0'-\frac{1}{2}\lambda)t]}{(\omega_0-\omega_0')}\sum_{n=1}^{+\infty}\left[\frac{i(\omega_0-\omega_0')}{b}\right]^n(tb)^{n/2}J_n(2b^{1/2}t^{1/2})\right|^2dx_1,$$

$$I(t)=E\int_0^{x_{1\,\max}}\frac{e^{-\lambda t}}{(\omega_0-\omega_0')^2}\sum_{n=1}^{+\infty}\sum_{m=1}^{+\infty}(-1)^n\left[i\frac{\omega_0-\omega_0'}{b}\right]^{n+m}(tb)^{(n+m)/2}J_n(2b^{1/2}t^{1/2})J_m(2b^{1/2}t^{1/2})dx_1.$$

When the integration with respect to x_1 is carried out, the following result is obtained:

$$I(t)=\frac{2\cos\Psi}{\cos\Psi+\cos\theta}Ee^{-\lambda t}t\left\{1-\sum_{n=1}^{+\infty}\sum_{m=1}^{+\infty}\frac{(i)^{n+m}(-1)^n}{(n+m-1)}[(\omega_0-\omega_0')(4t/B)^{1/2}]^{n+m-2}\right.$$
$$\left.\times[J_{n-1}(B^{1/2}t^{1/2})J_{m-1}(B^{1/2}t^{1/2})+J_n(B^{1/2}t^{1/2})J_m(B^{1/2}t^{1/2})]\right\},$$

where $B=rx_{\max}/c=r(x_{1\,\max}+x_{2\,\max})/c$, and θ and Ψ are the incidence and scattering angles with respect to the normal to the scatterer. This expression can be reduced to

$$I(t)=\frac{2\cos\Psi}{\cos\Psi+\cos\theta}Ee^{-\lambda t}t\left\{1-\sum_{N=0}^{+\infty}\frac{(-1)^{N+1}}{(2N+1)}\left[(\omega_0-\omega_0')^2\frac{4t}{B}\right]^N\sum_{m=1}^{2N+1}(-1)^m\right.$$
$$\left.\times[J_{2N+1-m}(B^{1/2}t^{1/2})J_{m-1}(B^{1/2}t^{1/2})+J_{2N+2-m}(B^{1/2}t^{1/2})J_m(B^{1/2}t^{1/2})]\right\}. \quad \text{(A6)}$$

This series converges rapidly for small values of $(\omega_0-\omega_0')^2 4t/B$.

For large values of $(\omega_0-\omega_0')^2 4t/B$ it is convenient to obtain $I(t)$ from the sum of (A3) and (A5):

$$I(t)=E\int_0^{x_{1\,\max}}\left|\frac{\exp\{i[\omega_0 t+b/(\omega_0-\omega_0')]-\frac{1}{2}\lambda t\}}{\omega_0-\omega_0'}-\frac{\exp[(i\omega_0'-\frac{1}{2}\lambda)t]}{\omega_0-\omega_0'}\sum_{n=0}^{+\infty}\left(\frac{i(b/t)^{1/2}}{\omega_0-\omega_0'}\right)^nJ_n(2b^{1/2}t^{1/2})\right|^2dx_1,$$

$$I(t)=E\int_0^{x_{1\,\max}}\frac{e^{-\lambda t}}{(\omega_0-\omega_0')^2}\left(1+\sum_{n=0}^{+\infty}\sum_{m=0}^{+\infty}(-1)^n\left(\frac{i(b/t)^{1/2}}{\omega_0-\omega_0'}\right)^{n+m}J_n(2b^{1/2}t^{1/2})J_m(2b^{1/2}t^{1/2})\right.$$
$$\left.-2\,\mathrm{Re}\left\{\exp\left[i\left(t(\omega_0-\omega_0')+\frac{b}{\omega_0-\omega_0'}\right)\right]\sum_{n=0}^{+\infty}\left(\frac{-i(b/t)^{1/2}}{\omega_0-\omega_0'}\right)^nJ_n(2b^{1/2}t^{1/2})\right\}\right)dx_1=I_1+I_2-I_3.$$

Reference 19 contains a series expansion for I_2. I_3 was evaluated from an expansion obtained by successive integrations by parts. This is done so as to obtain terms containing increasing powers of $(bt)^{1/2}$ and Bessel functions of increasing order. The final result thus obtained is

$$I(t)=\cos\Psi/(\cos\Psi+\cos\theta)\tfrac{1}{2}E[e^{-\lambda t}B/(\omega_0-\omega_0')^2]\{1+\sum_{N=0}^{+\infty}(-1)^N(\omega_0-\omega_0')^{-2N}(B/4t)^N$$
$$\times[(2N+1)^{-1}\sum_{m=0}^{2N}(-1)^m(J_m(B^{1/2}t^{1/2})J_{2N-m}(B^{1/2}t^{1/2})+J_{2N-m+1}(B^{1/2}t^{1/2})J_{m+1}(B^{1/2}t^{1/2}))$$
$$-[2(2N+2)/t(\omega_0-\omega_0')]\sin[B/4(\omega_0-\omega_0')+t(\omega_0-\omega_0')]J_{2N+2}(B^{1/2}t^{1/2})-4(2N+1)(Bt)^{-1/2}$$
$$\times\cos[B/4(\omega_0-\omega_0')+t(\omega_0-\omega_0')]J_{2N+1}(B^{1/2}t^{1/2})]\}. \quad \text{(A7)}$$

---

[19] Y. L. Luke, *Integrals of Bessel Functions* (McGraw-Hill Book Co., New York, 1962).